

# Geometric properties of deep-water breaking waves

By P. BONMARIN

Institut de Mécanique Statistique de la Turbulence, Unité Mixte Université/C.N.R.S.  
n° 380033, 12, Avenue du Général Leclerc – 13003 Marseille, France

(Received 6 July 1988 and in revised form 20 January 1989)

The time-space evolution of a steep water wave reaching the breaking stage is observed by means of a visualization technique. In particular, the asymmetry of the wave profile in the near-breaking region is displayed. Measurements at breaking onset on a sample of breaking waves show a relation between the rate of asymmetry growth and the breaker type. The shape evolution of a plunging crest after breaking has started, and the related splash-up phenomenon and its part in the air-entrainment process are also observed.

---

## 1. Introduction

There are a variety of reasons why breaking of waves is an important phenomenon. It has great significance in numerous aspects of air-sea interactions (energy transfer from wind to sea surface, horizontal momentum transfer from waves to surface currents, turbulent mixing of the upper marine layers, etc.). Breaking is responsible for the production of air bubbles and sea-water droplets which are important in consideration of the problems of heat and mass exchange across the sea surface. Spray ejection by the disengagement of entrained bubbles is a crucial factor in the far-field transport of pollution. The breaking process is a hydrodynamic source of underwater noise, and air bubbles a cause of disturbance for sound propagation. Other important consequences of breaking waves are the large hydrodynamic loads on coastal or offshore marine structures.

In view of this, there is a need for further basic understanding of the breaking process, up to and after the onset of breaking. Unfortunately, the study of breaking waves is difficult for several reasons. From a theoretical point of view, the equations of motion and also the boundary conditions are nonlinear; in addition, these conditions must be applied at the free surface whose location is not known beforehand. From an experimental point of view, observations and measurements are not easy for various reasons: breaking is an unsteady phenomenon occurring intermittently, starting suddenly and evolving rapidly; in addition, it presents three-dimensional and multiphase aspects. In the ocean, experimental conditions are particularly adverse, while in the laboratory, measurements cannot always be strictly extended to sea conditions because of the use of fresh water instead of salt water, and because they may not easily be scaled-up owing to the relatively great importance of surface tension and viscosity at small scale. The theoretical and experimental difficulties explain why the advance towards understanding the geometric, kinematic and dynamic properties of deep-water breaking waves has been relatively slow.

In recent years, numerical and mathematical models have made great strides compared to the early works of Biesel (1952) or Price (1971): the important stages

of this advance include especially the study of instability mechanisms and the simulation of wave overturning and incipient breaking (Longuet-Higgins & Cokelet 1976, 1978; Longuet-Higgins & Fox 1978; Cokelet 1979; Peregrine, Cokelet & McIver 1980; Vinje & Brevig 1981*a, b*; McIver & Peregrine 1981; Longuet-Higgins 1982; New 1983; Greenhow 1983; Kharif 1983; Schultz 1985; Jansen 1986*a*).

Experimentally, qualitative observations have been made on deep-water near-breaking waves that display a relatively good agreement with theoretical results; unfortunately quantitative results are not sufficient in number to make accurate comparison possible. Experiments have mainly concerned the shape evolution of waves approaching a beach: Mason (1952), Iversen (1953), Galvin (1968, 1972), and, more recently, Suhayda & Pettigrew (1977), Hansen & Svendsen (1979), Hotta & Mizuguchi (1980), Flick, Guza & Inman (1981), Hedges & Kirkgöz (1981), and lately Jansen (1986*b*).

On deep water, they have concerned especially the characterization of the instability mechanism leading to wave breaking, and the study of breaking criteria: Duncan (1981), Melville (1982), Su *et al.* (1982), Ramberg, Barber & Griffin (1985), Ramberg & Griffin (1986). Few experimental studies have been done on the near-breaking wave profile determination: among the recent publications those by Van Dorn & Pazan (1975), Van Dorn (1978), Kjeldsen & Myrhaug (1978) and Duncan (1981) are worthy of mention. Altogether, few quantitative results are available on the properties of deep-water breaking waves, and the aim of the present paper is to provide some.

There are two significant problems connected with the experimental determination of the shape of steep progressive waves: first, the continuous change of the profile in space and time; secondly, the number of parameters necessary to describe accurately the profile of an asymmetric wave. The shape of a steep progressive wave can change rapidly, especially during the near-breaking phase: the characteristic timescale can be of the order of  $T/10$ , where  $T$  is the wave period. In these conditions, measurement of the wave profile using classical fixed gauges becomes inaccurate, but visualization techniques are highly appropriate.

While two parameters, for example the amplitude and the wavelength, are enough for determining completely the shape of a sinusoidal wave, they are no longer adequate in the case of a steep asymmetric wave: indeed, several asymmetric waves can exist that have the same amplitude, or the same wavelength, or the same steepness, etc. Consequently, it is useful to introduce new parameters. Kjeldsen & Myrhaug (1978), the first to our knowledge, have defined such additional parameters (four in number) especially to specify the asymmetry of wave profile: a crest front steepness, a crest rear steepness, an horizontal asymmetry factor and a vertical asymmetry factor.

## 2. Experimental technique and procedure

The experiments were performed in the large air-sea interaction simulation facility of the IMST Laboratory, 40 m long, 3.20 m wide and 1 m deep. They concerned the shape evolution of steep deep-water waves up to and after the breaking stage. Deep-water conditions are realized in the tank because the water depth is of the same order as the maximum wavelength; consequently, the effect of the bed on the breaking process can be neglected.

In the present experiments, the wave profile was made visible by illuminating the water surface with a thin sheet of light, as indicated schematically in figure 1. Sharp

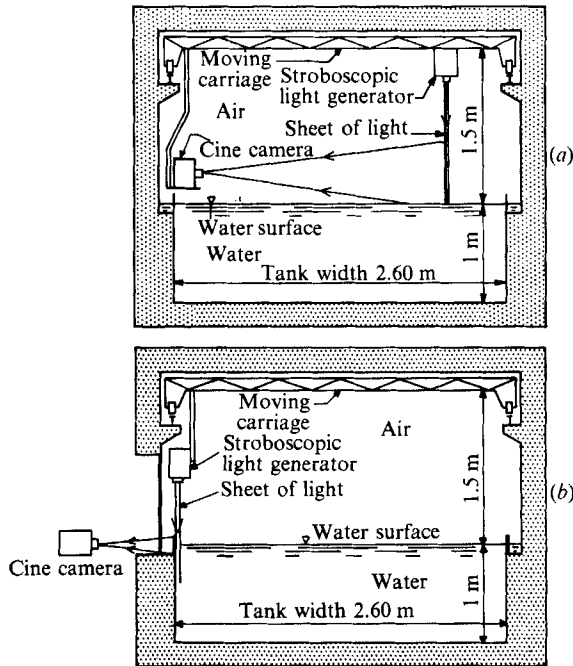


FIGURE 1. Principles of wave visualization and picture acquisition techniques. (a) Cine-movie camera moving at the phase celerity; (b) fixed cine-camera used for breaking process observation (light sheet thickness  $\approx 10$  mm).

pictures were obtained by using powerful flashing lamps synchronized either with a still camera or with a movie camera. Movie pictures were taken at different frequencies up to 300 frames per s, and stored on 16 mm films. As an illustration, a sample of two photographs and one still from a movie is shown in figure 2. Single images of the movie were manually digitized by means of a Hewlett-Packard 9874A digitizer. Each wave profile was transformed into a set of  $X$ - $Y$  coordinates, and the data (about 500 per wavelength) stored in a minicomputer for further processing.

Wavy motion of the water surface was produced by a completely immersed electro-hydraulic device capable of generating wave patterns in different modes: in particular either regular oscillations, in the frequency range from 1 Hz to 3 Hz (denoted as the first mode), or modulated oscillations (denoted as the second mode). In the first mode, breaking waves occurred inside wave trains generated by the growth of modulational instabilities on an initially unmodulated wave train (Benjamin-Feir instabilities). In the second mode, they occurred as the consequence of the dispersive property of surface waves by concentrating the energy of several successive waves at a same point. This effect was obtained by smoothly and slowly decreasing the frequency of the wave generator in order to create wave groups composed of waves with different celerities. The first mode allowed natural generation of spilling breakers as well as plunging breakers, while the conditions of the second mode were experimentally chosen in order to produce essentially plunging breakers. This last procedure was used for high-frame-frequency acquisitions. The experiments described in §§3.2, 4.1 and 4.2 used the first mode while the ones described in §4.3 used the second mode.

The measurements in §4.1 were made by following until the breaking stage the

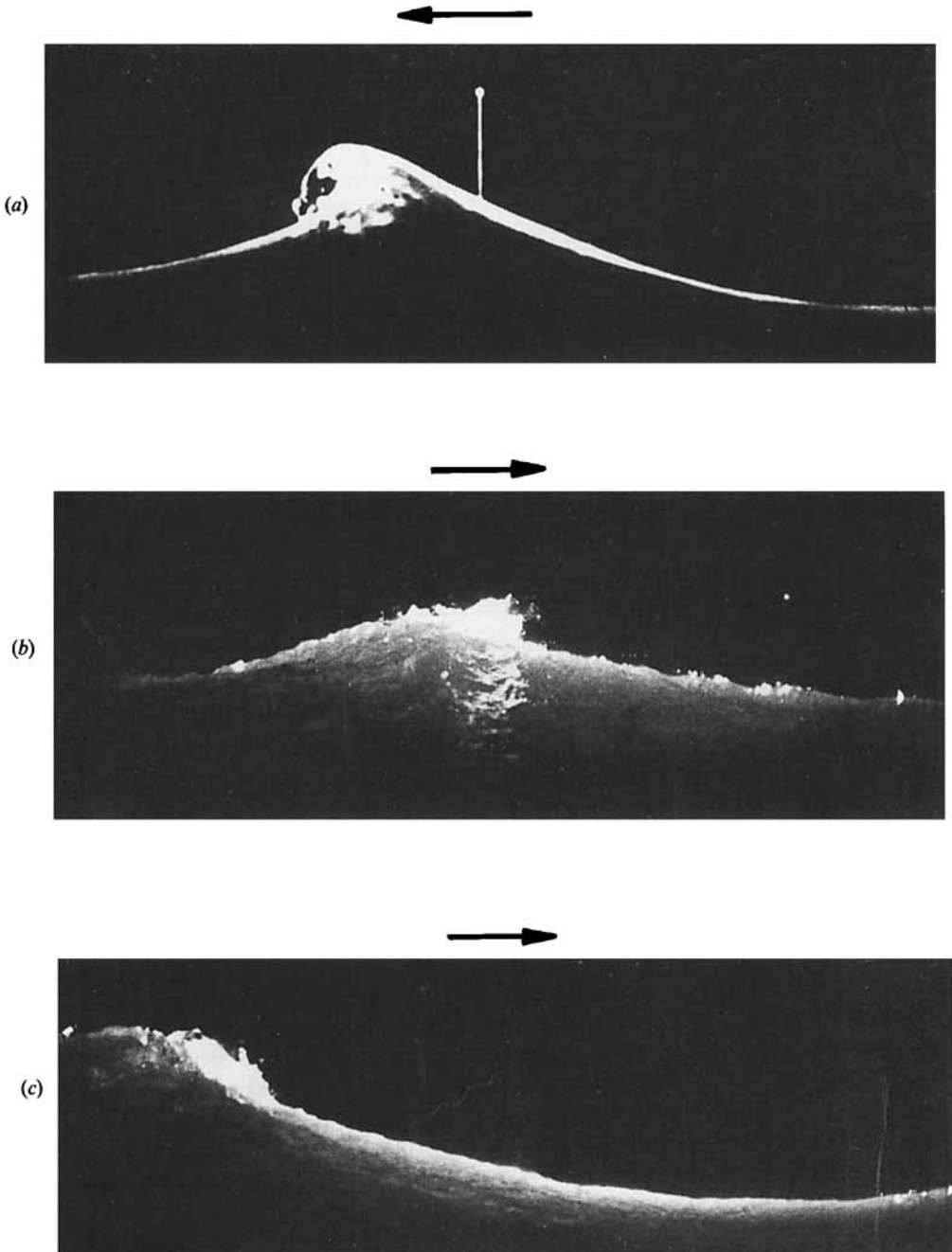


FIGURE 2. Sample of breaking waves: (a) plunging breaker (movie film; mechanical wave); (b) tearing of 'packets of sea' at the crest (photograph; wind  $14 \text{ ms}^{-1}$  over mechanical wave); (c) spilling breaker (photograph; wind  $14 \text{ ms}^{-1}$  over mechanical wave).

evolution of a progressive wave of initial steepness equal to 0.28, near to but less than the value 0.29 that marks the limit of a regime where the Benjamin–Feir instability dominates and where consequently the approach to breaking is essentially two-dimensional (Longuet-Higgins & Cokelet 1978; Melville 1982), as opposed to a regime where the Benjamin–Feir instability is dominated by a three-dimensional instability, leading to breaking, which appears for an initial steepness greater than 0.31 (Melville 1982).

This steepness allowed the generation of a relatively high wave still consistent with a two-dimensional aspect, and of a long length which nevertheless was inside the camera field. A height and a length maximum were desirable so give an accuracy maximum in image analysis.

The present experiments were conducted without wind so that this initial study could be of a simple situation with two-dimensional waves. It is nevertheless true that on the ocean wind can play a dominant role in the generation and development of the breaking process through the shearing stress and the normal pressure, and further studies should take these roles into consideration.

The camera was placed either at a fixed location or on a moving carriage transported at a constant speed close to the phase celerity. This last procedure allowed progressive waves to be followed and thus observations of wave evolution during several periods up to the breaking stage could be made.

### 3. Experimental data

#### 3.1. Wavelength definition

The measurements and calculations used the following wavelength definition: the initial still-water surface being considered as a reference level, a single wave is defined as the surface profile between one point where the water surface intersects with the still water level with a negative gradient before the trough, and the first following point where the surface profile again intersects with the still water level with a negative gradient (see figure 3). Such a definition of a single wave is known as the ‘zero-downcross analysis’. A ‘zero-cross analysis’ definition was chosen because it allows a more accurate measurement of the wavelength on the pictures than a method consisting, for example, of measuring the distance between two successive crests: the intersection between the two lines representing respectively on the pictures the mean water level and the wave profile is more accurate than the location of a crest when this latter displays a smooth shape. The ‘zero-downcross analysis’ is sometimes chosen because, with this definition of wave height, a parameter is obtained that is very relevant to the analysis of capsizing of vessels and of shock pressures on fixed structures, which are obviously important from a practical point of view.

#### 3.2. Breaking criterion definition

The onset of breaking was determined by means of an easily observed visual criterion in the movie pictures: for a plunging breaker, it corresponds to the occurrence of a vertical crest front, for a spilling breaker, it corresponds to foam occurrence.

This criterion has been compared to experimental breaking criteria obtained relatively recently by different authors and collected by Ramberg & Griffin (1986) (figure 4 and table 1). They present these criteria as a relation between the wave height  $H$  and a period parameter  $gT^2$ , where  $T$  is the wave period and  $g$  denotes the acceleration due to gravity. Ramberg & Griffin compare the wave height to a theoretical limiting wave height  $H = 0.027gT^2$  which is based on the classical relation



$H = 0.141L_*$ , where  $L_*$  denotes the Stokes limiting wavelength, approximated here to the second order by the relation  $L_* \approx 1.2gT^2$ .

The present results, like those from other researchers, show clearly that the limiting wave steepness at breaking inception is less than the theoretical Stokes limit  $0.027gT^2$  introduced by Ramberg & Griffin.

It should be noted here that the experiments by Ochi & Tsai (1983), as the present observations, concerned breaking processes initiated by natural modulations of initially two-dimensional waves in facilities of constant width and depth, while Duncan's observations concerned steady breakers produced by towing an hydrofoil just beneath the surface, and in Ramberg & Griffin's experiments breakers were caused by the creation of a convergent zone. In spite of the different ways used to produce the breaking waves on deep water, plunging as well as spilling breakers from different origins appear to present qualitatively similar properties. As could be expected, the scattering of the results is slightly larger for the natural waves than for the artificial ones.

In addition, the present observations show that the breaking coefficient  $\sigma' = H/gT^2$  depends on the breaker type, the highest values corresponding to the typical plunging breakers; but the difference is not sufficiently marked for this coefficient to be an accurate means of breaker classification.

## 4. Results

### 4.1. Wave evolution to breaking

In spite of the fact that both plunging and spilling breakers exist in the ocean, observations have been focused on the plunging breaker which is the most powerful breaker in deep and in shallow water, and which plays a particularly active role in air-sea interactions, especially for mass transfer phenomena across the water surface (Merlivat & Memery 1983).

During the period preceding breaking, the wave profile becomes more and more asymmetric, particularly near the crest, the trough maintaining its smooth and regular initial form to a first approximation, as illustrated in figure 5. Experiments were performed with the intention of measuring the shape evolution of a progressive wave up to the onset of breaking. In these experiments, the profile of the waves was defined by 37 geometric parameters or coefficients. In addition, eight parameters were defined in relation to the potential energy (see table 2).

An endless list of parameters could be established but in order to keep the list down to a manageable size, in the present paper, only seven geometric parameters and two coefficients related to potential energy, among the ones mentioned above, have been considered. These parameters and coefficients have been chosen because they provide information about the wave characteristics most useful from a theoretical and a practical point of view.

In the present experiments, the breaking process generated by the first mode resulted from the natural deformation of a progressive mechanical wave becoming more and more steep. A sample of results so obtained is presented now: it refers to the chronological series of wave profiles displayed in figure 5. For typical plunging breakers, qualitative analysis of several chronological series of pictures having shown that the evolution of waves in the near-breaking region look similar, and also because of the relative awkwardness of the semi-manual image analysis process, detailed quantitative measurements were made on three chronological series of cine movie

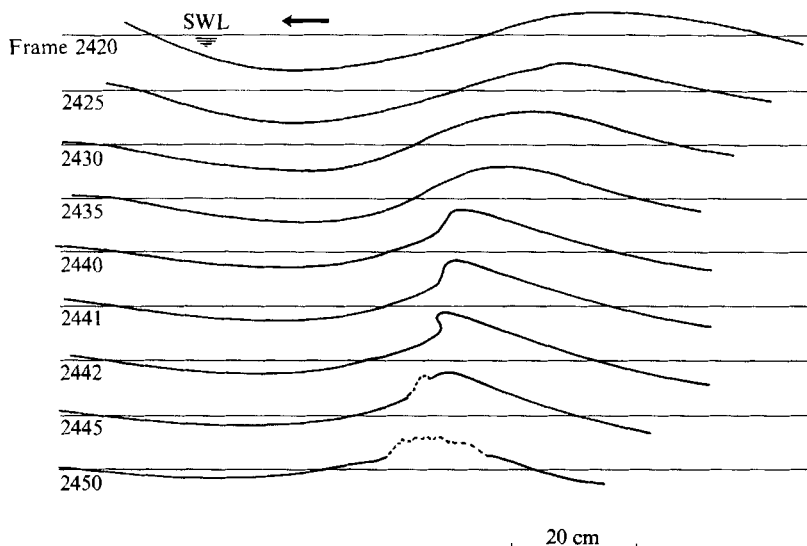


FIGURE 5. Evolution of a steep mechanical wave reaching the plunging stage, from the cine film analysis. Frame frequency,  $24 \text{ f s}^{-1}$ .

---

Parameters related to the whole wave

- $L$  Total wave length  
 $H$  Total wave height  
 $\gamma$  Wave steepness  $\gamma = H/L$   
 $\mu$  Horizontal asymmetry factor  $= \eta'/H$  (describing the wave asymmetry with respect to an horizontal axis: still-water level (SWL))  
 $E_p$  Potential energy of the wave/ $L$ , along 1 m of crest

Parameters related to the crest

- $\eta'$  Crest elevation above still water level  
 $\lambda$  Vertical asymmetry factor  $= F_2/F_1$  (describing the crest's asymmetry with respect to a vertical axis through this latter)  
 $\epsilon$  Crest front steepness  $\epsilon = \eta'/F_1$   
 $\delta$  Crest rear steepness  $\delta = \eta'/F_2$   
 $\gamma'$  Crest steepness  $\gamma' = \eta'/L$   
 $E_+$  Potential energy located in the crest/ $L_2$ , along 1 m of crest  
 $e_+$  Ratio between the potential energy in the crest and the potential energy in the whole wave  
 $\alpha_1$  Crest front angle  
 $\alpha_2$  Crest rear angle

Parameters related to the trough

- $\eta''$  Trough depression below still water level  
 $\gamma''$  Trough steepness  $\gamma'' = \eta''/L$   
 $E_-$  Potential energy located in the trough/ $L_1$ , along 1 m of crest  
 $e_-$  Ratio between the potential energy in the trough and the potential energy in the whole wave  
 $\alpha'_1$  Trough front angle  
 $\alpha'_2$  Trough rear angle

TABLE 2. Definition of wave parameters (partial list)

---

pictures. The quantitative results were sufficiently similar that only one sample of results is presented here.

Observations were made by means of a cine camera moved with a constant speed corresponding to the phase celerity of a first-order wave of  $T_0^{-1}$  frequency, where  $T_0$  is the wavemaker period. In order to take into account the continuous change of the phase celerity of the steep progressive wave observed, and because a complete wavelength must be always visible inside the field of the camera, this field must be sufficiently larger than the wavelength of the observed wave. Since the camera frequency was strictly constant and known, the time step between the successive frames was consequently well determined and measurements of the time evolution of the waves characteristics were possible.

The first parameter considered was the wavelength. A regular decrease of this parameter was observed up to the plunging point (see figure 6). This decrease of the wavelength can lead to a modification of the crest frequency. It will be shown later (§4.3) that such a modification might also be caused by phenomena occurring during the breaking process itself (splash-up occurrence and disappearing of the original breaking crest).

The crest elevation and the trough depth have similar values, expressing the relative initial symmetry of the wave; then they reach maximum values, located at breaking onset for the crest elevation, and significantly before this stage for the trough depth (see figure 7). Close to breaking an increase of the crest elevation occurs simultaneously with a decrease of the trough depth.

A similar tendency was observed on theoretical profiles computed by Longuet-Higgins & Cokelet (1978): on the profiles of a steep progressive wave with initial steepness of the same order as the present one (0.25 compared to 0.28), a ratio higher than 1 ( $\approx 1.2$ ) was indeed measured between the crest elevation at a time very close to breaking onset and a short time before, while a ratio less than 1 ( $\approx 0.8$ ) was observed for the trough depth. The present comparison between experiment and theory based on measurements on two theoretical profiles in the near-breaking region must be considered as a first step because of the restricted number of profiles taken into consideration; an extensive and more significant comparison should cover the complete series of theoretical profiles up to breaking onset.

The evolution of the wave from an initial symmetric form to an asymmetric one, as it progresses towards the breaking stage, is also clearly displayed by the measurements of the two asymmetry factors  $\mu$  and  $\lambda$  defined in table 2. Initially the horizontal asymmetry factor  $\mu$  is close to the value 0.5 corresponding to a symmetric wave. It suddenly increases and reaches a value close to 0.90, expressing a high level of asymmetry (see figure 8). A comparison between figures 7 and 8 shows a correlation between the evolution of the horizontal asymmetry factor and the trough depth  $\eta''$ ; each of these evolutions indicates clearly the transition from a symmetric state to an asymmetric one (close to frame number 2423).

The crest also presents a high asymmetry relatively to a vertical axis, as shown in figure 9. This asymmetry results from the increase of the crest front slope, which is expressed by the evolution of the crest front steepness (see figure 10).

Although the crest front steepness variation is relatively large, the variation of the rear crest steepness is relatively small: it has been observed that this parameter increases slightly and remains between 0.20 and 0.35: thus the crest deformation results essentially from the crest front steepness increasing.

The observed increase of the asymmetry factors  $\mu$  and  $\lambda$  and of the two steepnesses  $\epsilon$  and  $\delta$  is in agreement with the evolutions measured on the theoretical profiles

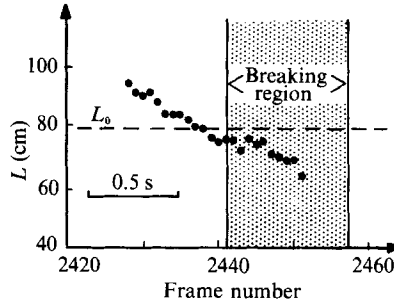


FIGURE 6. Time evolution of the wavelength. Frame frequency,  $24 \text{ fs}^{-1}$ ;  $L_0$ , length of a sinusoidal wave at the frequency  $T_0^{-1}$  ( $T_0$ , period of the wavemaker).

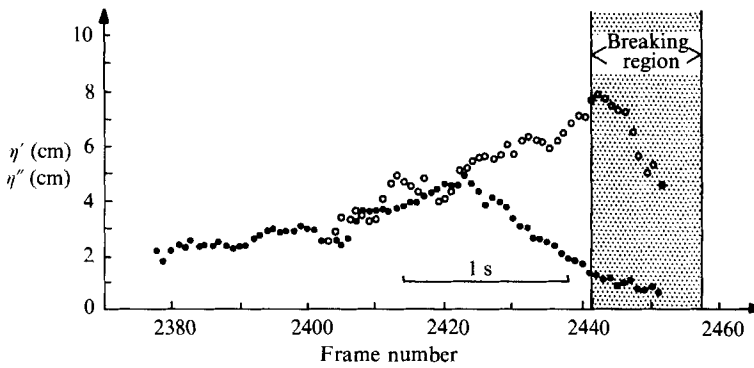


FIGURE 7. Time evolution of the crest elevation,  $\eta'$  (○), and of the trough depth,  $\eta''$  (●); frame frequency,  $24 \text{ fs}^{-1}$ .

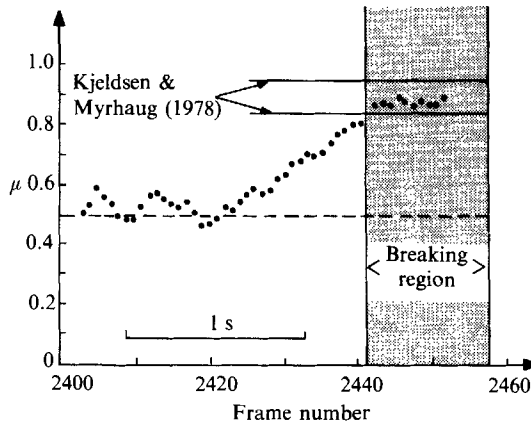


FIGURE 8. Time evolution of the horizontal asymmetry factor. ---, Symmetric wave; —, limit values observed by Kjeldsen & Myrhaug (1978); frame frequency,  $24 \text{ fs}^{-1}$ .

obtained by Longuet-Higgins & Cokelet: indeed measurements on these profiles give respectively  $\mu \approx 0.77$ ,  $\lambda \approx 1.8$ ,  $\epsilon \approx 0.59$  and  $\delta \approx 0.32$  at breaking onset, and  $\mu \approx 0.71$ ,  $\lambda \approx 1.8$ ,  $\epsilon \approx 0.48$  and  $\delta \approx 0.26$  a short time before ( $\approx T/4$  before, where  $T$  is the unperturbed wave period).

A final remark about the comparison between theory and experiment concerns the

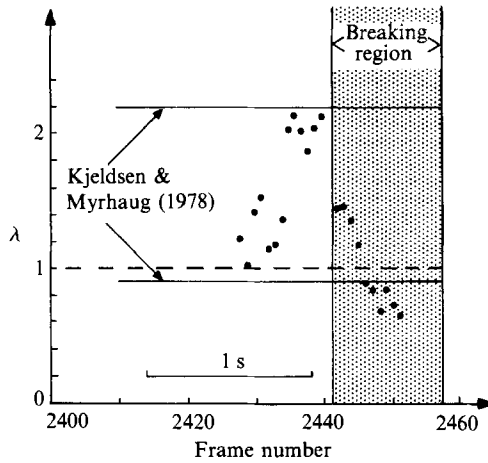


FIGURE 9. Time evolution of the vertical asymmetry factor. ---, Symmetric wave; —, limit values observed by Kjeldsen & Myrhaug (1978); frame frequency,  $24 \text{ f s}^{-1}$ . (The crest, as defined by zero-downcross analysis, appears for the first time in the camera field at frame 2428.)

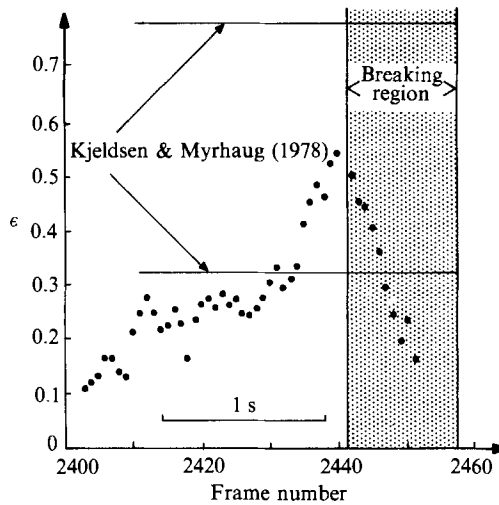


FIGURE 10. Time evolution of the crest front steepness. —, Limit values observed by Kjeldsen and Myrhaug (1978). Frame frequency,  $24 \text{ f s}^{-1}$ .

wavelength evolution. If in the computation by Longuet-Higgins & Cokelet the wavelength of the perturbation remains constant, that of the breaking wave included inside this constant wavelength changes with time. While measurement of the wavelength, made by the zero-downcross analysis method on the two theoretical profiles and separated by a short time interval, displays no significant evolution (a decrease of about 3%), there appears on the other hand to be a decrease of about 11% between the length of the breaking wave measured at the initial time  $t = 0$  (before the application of the perturbation) and its length at breaking onset.

In conclusion, the embryonic comparison between theory and experiment presented above displays on the whole a satisfactory qualitative agreement. It will be shown in §4.2 that quantitative agreement was also obtained to a first approximation.

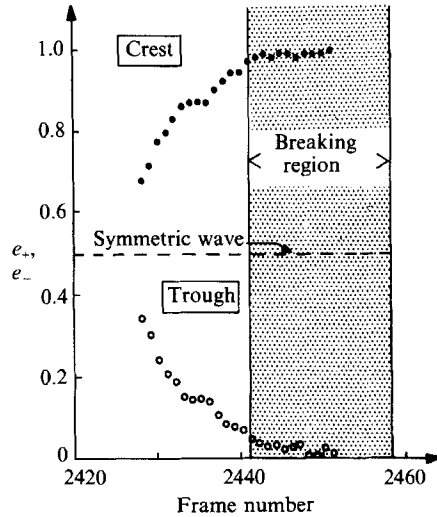


FIGURE 11. Time evolution of the ratio between the potential energy located in the crest, and in the trough, and the total potential energy of the wave. Frame frequency,  $24 \text{ f s}^{-1}$ .

The deformation of the wave profile leads to an evolution of the potential energy distribution. Thus as the wave progresses towards the breaking stage, the potential energy tends to concentrate into the crest (see figure 11).

The results presented above show how some geometric properties of a breaking wave, and especially of a breaking crest, can change significantly during the prebreaking phase and reach limit values at breaking onset. Breaking onset appears to be a transient phase and the aim of the results presented below is to define precisely the wave form at this stage of its evolution.

#### 4.2. Geometrical properties at breaking onset

Measurements were made on a sample comprising one hundred crests and eighty complete wavelengths. Since the observed breakers did not correspond exactly to the theoretical definitions of plunging breakers or of spilling breakers, we classified them into five categories as indicated in table 3. The adopted classification is based on the following subjective criterion: the breakers that display very distinctly all the characteristics of the theoretical plunging definition are called 'typical plunging breakers', as opposed to the ones where the plunging effect is only distinctly dominating; a parallel criterion was applied to the case of the spilling breakers.

The observations previously described here demonstrated that the wave profiles became asymmetric in the near-breaking zone, the asymmetry becoming more and more marked as the wave comes up to the breaking stage. At breaking onset, the horizontal as well as the vertical asymmetry can be very pronounced as indicated by the limit values reached by the horizontal asymmetry factor  $\mu$ , and by the vertical asymmetry factor  $\lambda$  (see tables 4a and 4b). The rate of asymmetry growth for  $\mu$  can be estimated by comparison with the value 0.5, and for  $\lambda$  this rate can be estimated in the same way by comparison with the value 1. The asymmetry of the crest can be estimated by comparing the measurements of the crest front steepness  $\epsilon$  with those of the crest rear steepness  $\delta$  (see tables 4c and 4d). The data presented corroborate the general observation concerning breaking waves, and especially plunging breakers, of a front crest steeper than the rear crest.

Breaker type	Symbol	Relative number (%)
Typical plunging breakers	1*	12
Plunging breakers	1	31
Typical spilling breakers	2*	8
Spilling breakers	2	19
Unclassified	0	30

TABLE 3. Definition of breaker types

Breaker type	Minimum value	Maximum value	Mean value	Symmetric wave
<i>(a)</i> $\mu$				
Typical plunging	0.65	0.93	0.77	0.5
Plunging	0.62	0.93	0.76	0.5
Spilling	0.59	0.91	0.75	0.5
Typical spilling	0.60	0.80	0.69	0.5
<i>(b)</i> $\lambda$				
Typical plunging	0.97	3.09	2.14	1
Plunging	0.78	2.52	1.61	1
Spilling	0.78	2.37	1.38	1
Typical spilling	0.81	1.72	1.20	1
<i>(c)</i> $\epsilon$				
Typical plunging	0.31	0.85	0.61	—
Plunging	0.29	0.77	0.47	—
Spilling	0.24	0.68	0.41	—
Typical spilling	0.31	0.51	0.38	—
<i>(d)</i> $\delta$				
Typical plunging	0.24	0.33	0.29	—
Plunging	0.20	0.42	0.30	—
Spilling	0.19	0.42	0.31	—
Typical spilling	0.26	0.48	0.33	—
<i>(e)</i>				
Parameters	$\mu$	$\lambda$	$\epsilon$	$\delta$
Theory ( $ak_{\text{initial}} = 0.25$ )	0.77	1.83	0.59	0.32
Present experiments ( $ak_{\text{initial}} \approx 0.28$ )	0.76	1.76	0.51	0.30
Symmetric wave	0.5	1	0.282*	0.282*

\* The value 0.282 corresponds to a second-order Stokes wave of steepness  $\approx 0.141$ .

TABLE 4. *(a)* Horizontal asymmetry factor  $\mu$ ; *(b)* vertical asymmetry factor  $\lambda$ ; *(c)* crest front steepness  $\epsilon$ ; *(d)* crest rear steepness  $\delta$ . *(e)* Degree of asymmetry of a plunging crest: comparison between theory and experiment.

The degree of asymmetry of the crest observed experimentally during the present experiments, and expressed by the two factors  $\mu$  and  $\lambda$ , and by the two steepnesses  $\epsilon$  and  $\delta$ , has been compared to that of the plunging breaker obtained theoretically by Longuet-Higgins & Cokelet (see §4.1). Table 4(e) displays this comparison. The experimental results presented in the table correspond to mean values computed on the sample of breakers composed by the reunion of plunging breakers of type 1 and 1\* previously defined (table 3). It will be noticed that the degree of asymmetry of the theoretical profile and that obtained experimentally are of the same order to a first

---

Breaker type	$\left(\frac{\alpha_1}{\alpha_2}\right)$ (crest)	$\left(\frac{\alpha'_1}{\alpha'_2}\right)$ (trough)
Typical plunging	0.80	1.02
Plunging	0.89	1.01
Spilling	0.93	1.01
Typical spilling	0.97	0.99

---

TABLE 5. Comparison between crest and trough angles

approximation. This relatively good agreement between theory and experiment, added to that previously observed in §4.1, can be considered as an indication of the realistic properties of the computation. Obviously further comparisons would be necessary to confirm definitively this opinion.

The trough of the breaking wave displays a relative symmetry compared to the asymmetry of the crest as indicated by the data in table 5. It will be observed that whatever the breaker type may be the angle  $\alpha'_1$  is of the same order as  $\alpha'_2$ , expressing the symmetry of the trough. On the other hand, the angle  $\alpha_1$  is always less than  $\alpha_2$ , expressing the asymmetry of the crest relatively to a vertical axis.

It has been shown previously that the potential energy of the wave tended to concentrate into the crest as the wave progressed towards the breaking point. This phenomenon is confirmed by measurements made at breaking onset (see figure 12). Thus, 75% of the breaking waves (all breaker categories mixed) show a ratio between the potential energy located in the crest and the potential energy located in the whole wave of higher than 0.80 (see figure 12*b*). The opposite tendency is observed for the energy located in the trough: about 75% of the breaking waves show a ratio between the potential energy located in the trough and the potential energy located in the whole wave of less than 0.20 (see figure 12*c*). Such a distribution could derive from the mixing of different breaker categories (from typical plunging to typical spilling) and also from differences in the degree of asymmetry of the waves at breaking onset.

In addition to the display of a relatively marked asymmetry of the wave at breaking onset, the measurements presented above show a relation between the rate of asymmetry growth and the breaker type: the maximum asymmetry corresponding to the typical plunging breakers, the minimum corresponding to the typical spilling ones. The measurements have shown that the tendency of the wave potential energy to concentrate into the crest is more marked for a plunging wave than for a spilling one (see figure 13).

#### 4.3. Crest evolution after breaking onset

For the plunging type, considered in particular here, the whole front face of the crest steepens, becomes vertical, and a jet of water is projected forward into a characteristic overturning motion (see figures 14 and 15). As the falling jet hits the undisturbed water surface in front of the crest, some water splashes up.

From the first splash-up so generated onward, the breaking process generally displays a chaotic aspect corresponding to a turbulent motion of mixed air and water, the toe of this chaotic flow progressing forward like a bore. Sometimes, however, it can display relative order by generating successive vortices, as it will be discussed later on.

Schematically, the plunging process can hence be decomposed into three stages: a first one corresponding to the formation of an overturning motion; a second to the

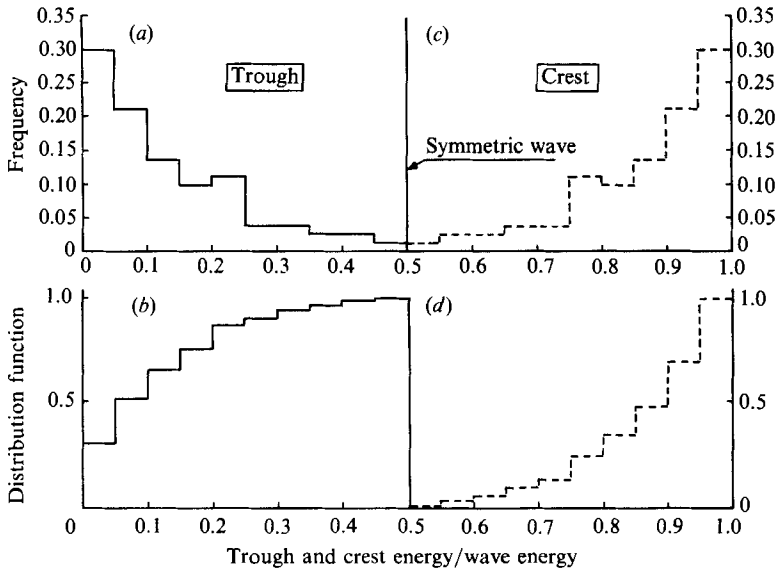


FIGURE 12. Histograms (*a, b*) and distribution functions (*c, d*) of the ratio between the potential energy located in the trough, and in the crest, and the potential energy in all the wave (all breaker categories mixed).

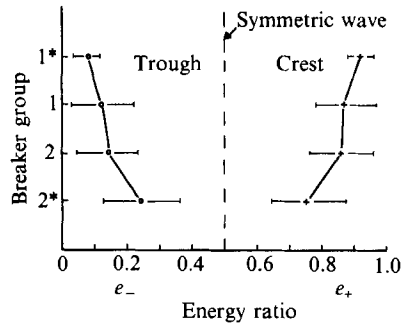


FIGURE 13. Influence of the breaker type on the ratio between the potential energy located in the crest, and in the trough, and the potential energy in all the wave (the mean values of the ratio and the standard deviations are plotted).

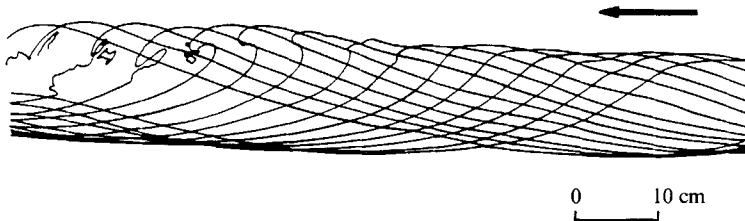


FIGURE 14. Observed crest deformation of a plunging breaking wave (observation interval  $\approx 0.04$  s).

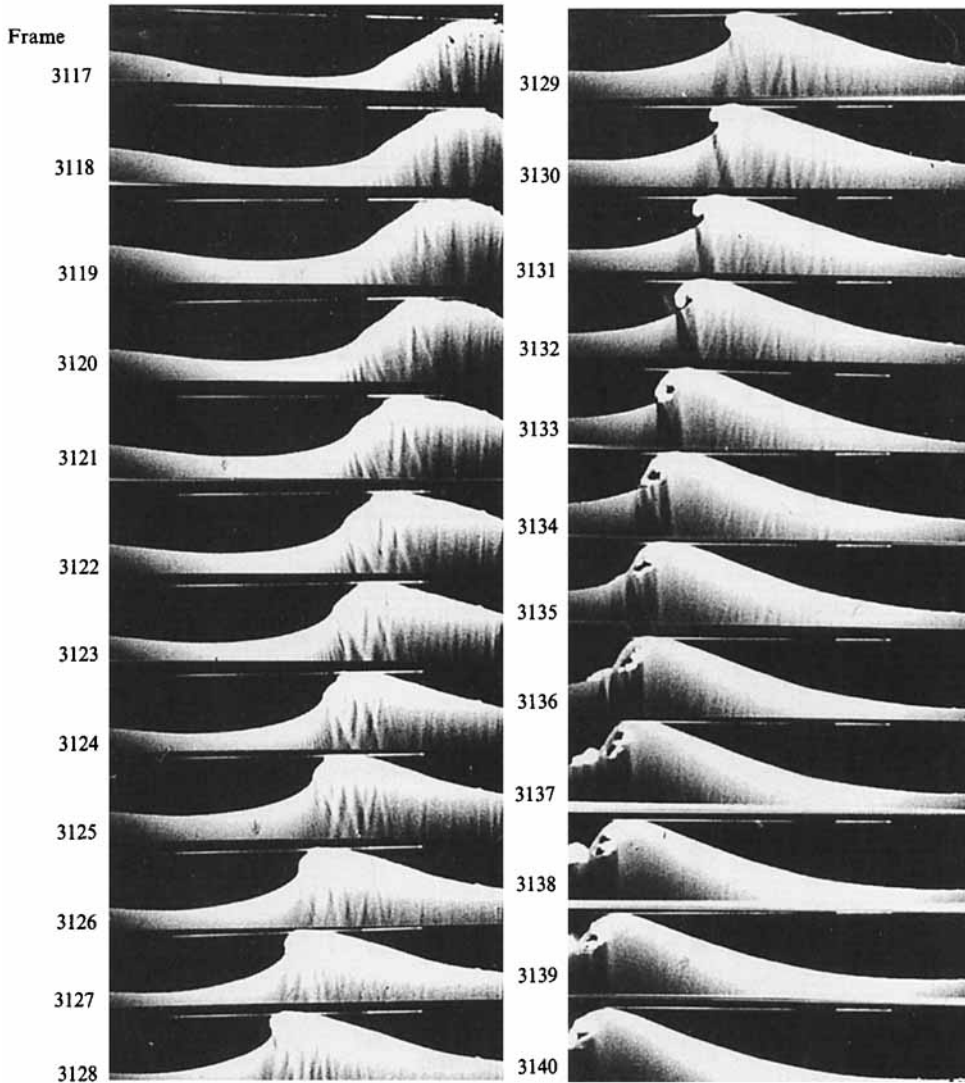


FIGURE 15. Chronological series of movie pictures showing the crest deformation preceding and during the plunging process, and the splash-up occurrence (interframe time  $\sim 0.04$  s (Film BUL 11)).

occurrence of one or several successive large and evolving splash-ups of water; a third to a degenerated and chaotic motion (see figure 16).

#### 4.3.1. *The overturning phenomenon*

Until the last few years, no satisfactory mathematical solution was available for describing the crest overturning phenomenon. Recently, substantial progress has been made in this direction: Longuet-Higgins (1982) showed that a class of cubic flows had a free surface corresponding to the forward face of a plunging breaker, while New (1983) showed that a certain region of the surface profile beneath the overturning crest of a plunging breaker was well approximated by an ellipse with axes in the ratio  $\sqrt{3}$ . On the other hand, Longuet-Higgins (1980, 1983) described a model valid for the jet of fluid ejected from the top of the plunging crest.

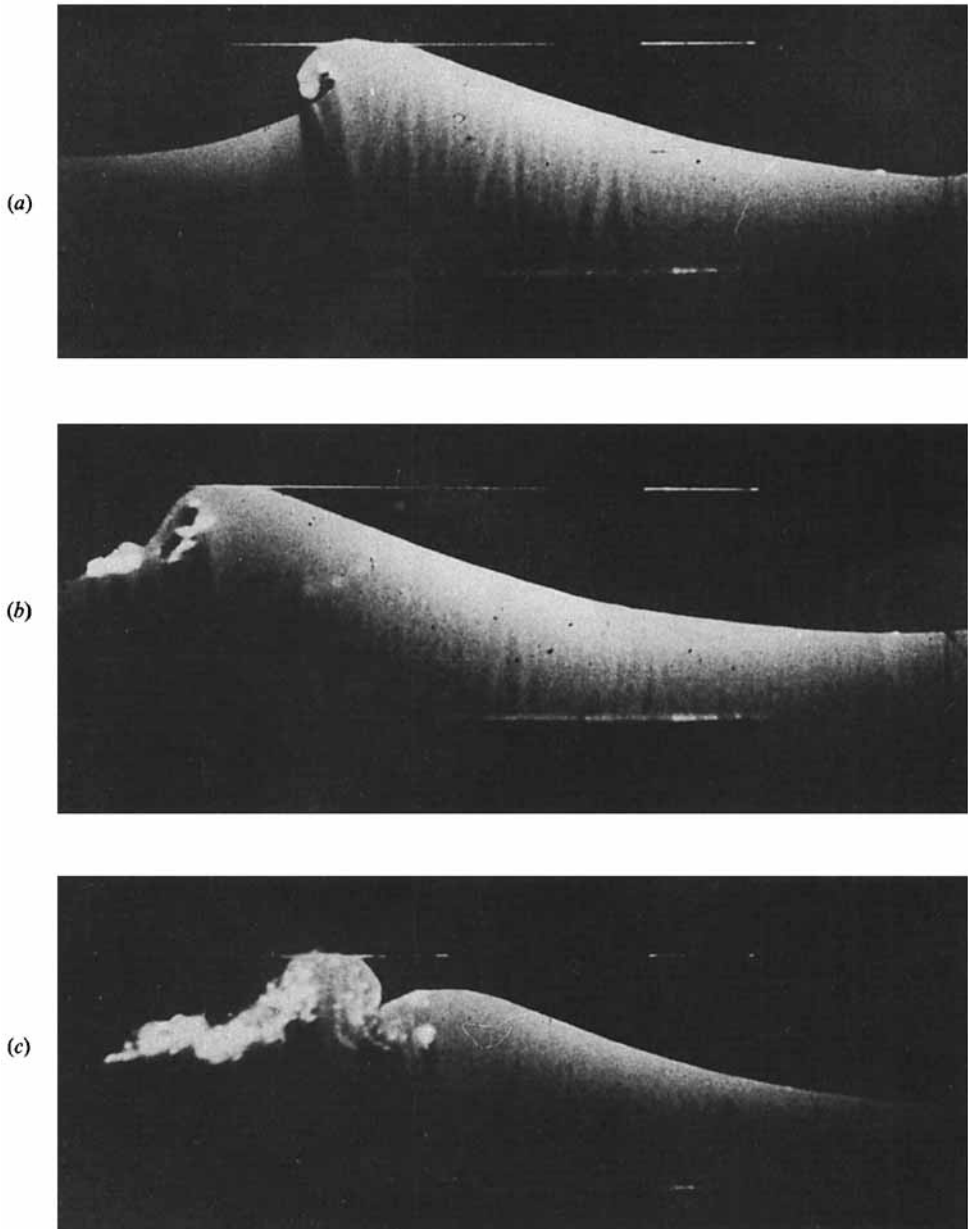


FIGURE 16. The three stages observed during the plunging process: (a) falling jet; (b) splash-up occurrence; (c) chaotic air-water motion.

Unfortunately both these models accounted for only a limited part of the wave profile and not the entire overturning region. An advance was made by Greenhow (1983) who suggested a solution combining both the ellipse model of New and the jet model of Longuet-Higgins. This solution is relevant at the jet and around the loop of the wave, not too far from the wave crest.

The ellipse solution of New has been tested experimentally on a series of movie pictures showing the time evolution of a plunging crest. The comparison displays a relative good agreement as indicated in figures 17 and 18.

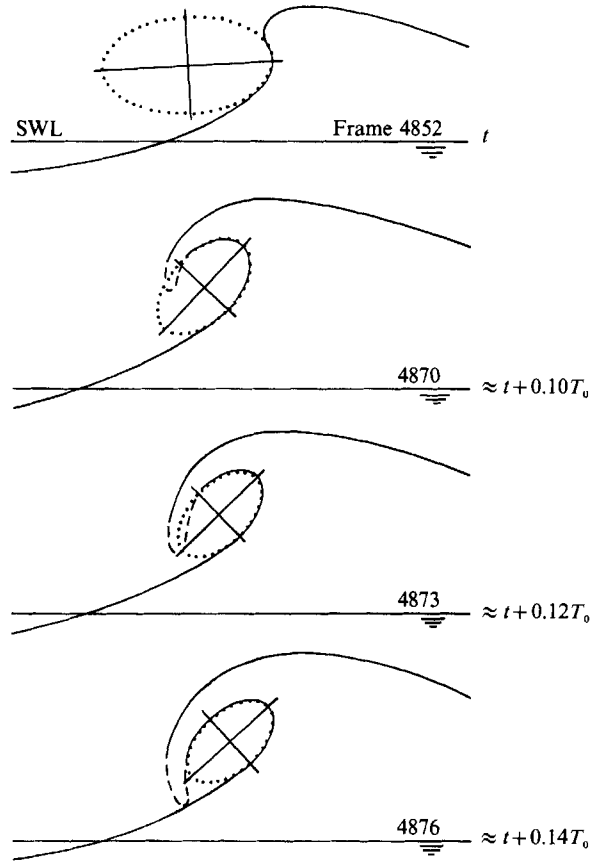


FIGURE 17. Fits of ' $\sqrt{3}$  aspect-ratio' ellipses to observed profiles.  $T_0$ , wavemaker period (cine camera frequency,  $200 \text{ f s}^{-1}$ ).

For each picture, the ellipse chosen was the one displaying the most accurate fit along the largest portion of the underside of the breaking crest. This most accurate fit was determined visually by successive approximations. As indicated by New, one can observe that the more the wave develops, the closer the underside of the breaking crest becomes to a  $\sqrt{3}$ -aspect-ratio ellipse.

#### 4.3.2. *The splash-up phenomenon*

The first splash-up occurring after the collision between the falling water jet and the undisturbed water surface develops and can display a structure schematically composed of two large vortices, one revolving clockwise, the other anticlockwise, as indicated in figure 19. At first, the occurrence of the splash-up does not appear to disturb the original breaking crest progression, as if this phenomenon, at least initially, was a minor surface event. However, it will be observed later (§4.3.3) that the splash-up occurrence coincides with the incipient decreasing of the original breaking crest celerity, meaning that the advent of this phenomenon does affect the wave progression.

After the first splash-up, the flow can either directly degenerate into a chaotic motion or display a relative order in the form of successive splash-up cycles and vortices which are less and less active (see figure 20). In this case, large coherent

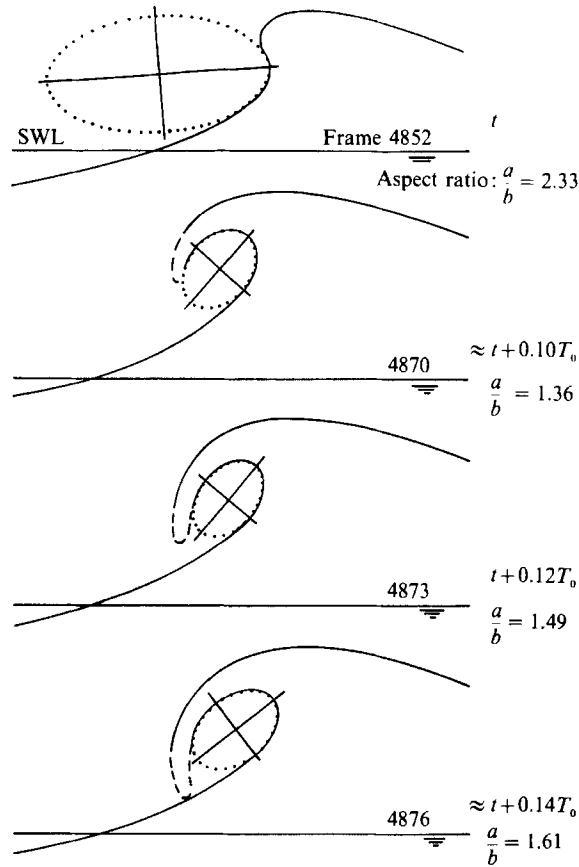


FIGURE 18. Best-fitted ellipses on observed profiles.  $T_0$ , wavemaker period. The dashed line corresponds to regions where droplets and foam make the water jet profile uncertain (cine camera frequency,  $200 \text{ f s}^{-1}$ ).

motions under the water surface have been observed by means of the small entrained air bubbles as tracers. In shallow water the development of such coherent structures have been displayed by Jansen (1986*b*): this author also observed that particle trajectories were smooth in certain zones inside the jet splash.

No clear explanation can be given on the mechanism responsible for the splash-up formation. In particular the origin of the emerging water is not clear: Peregrine (1983) has proposed three schemes for explaining this phenomenon (see figure 21), but visual and photographic observations are not sufficiently numerous or clear for deciding with assurance. It appears clearly from our own observations, based on slow film motion analysis, that the falling water jet penetrates the surface generating large eddies, as schematically indicated in figures 19 and 20. This penetration, and the development of a large eddy under the water surface (moving anticlockwise in the above-mentioned figures), seems rather inconsistent with a process such as (a) in figure 21.

On the other hand, a wedge of clear water free of air bubbles, previously observed in shallow water (Peregrine 1983), appears inside the splash-up (see figure 22), and the cine movie shows that, at least initially, it moves as if it were pushed up and forward by the falling water jet: this latter acts at that time like a solid wedge. In

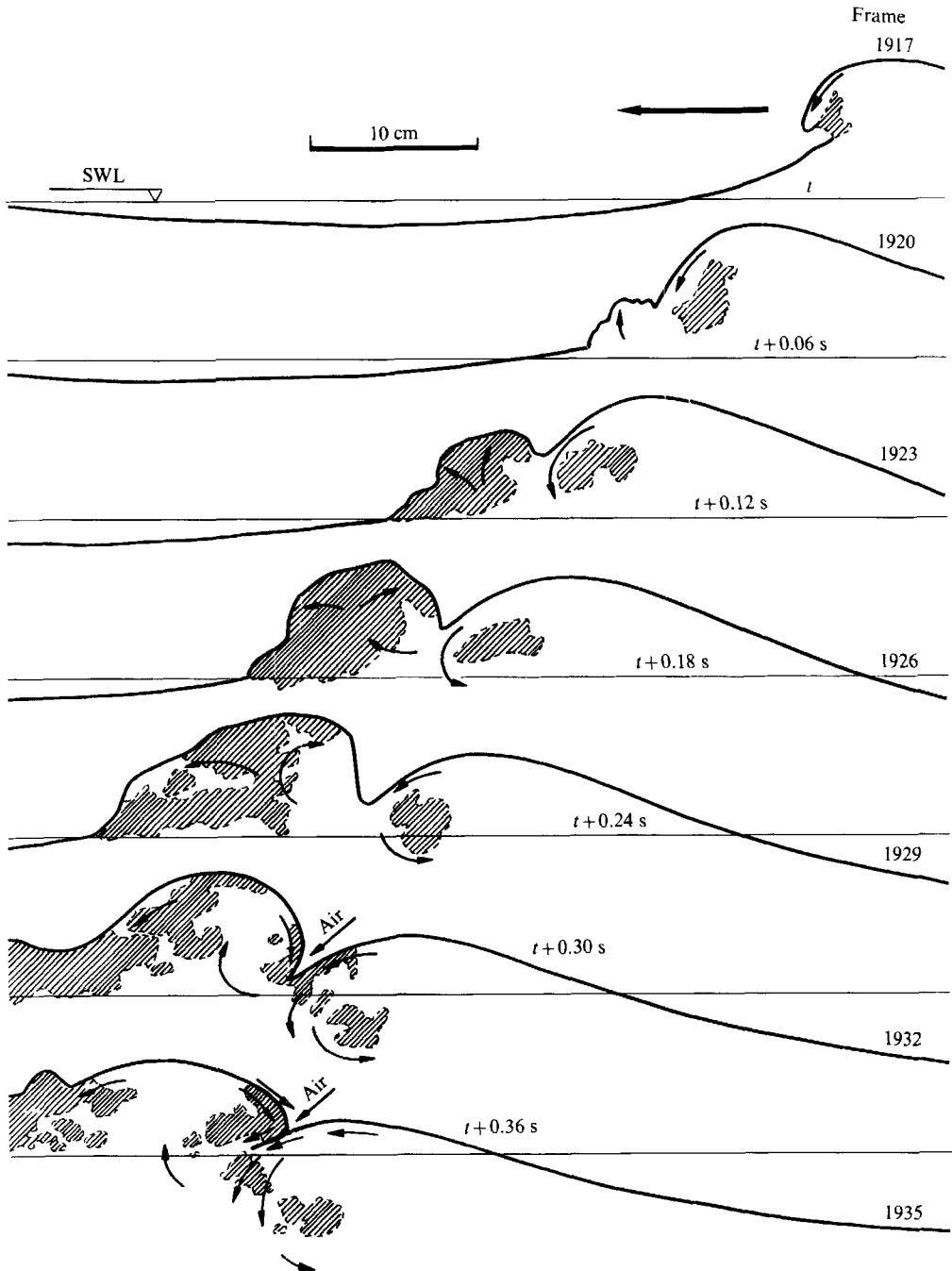


FIGURE 19. Chronological reconstruction of the splash-up occurrence and schematic view of the large underwater structures (cine camera frequency,  $24 \text{ f s}^{-1}$ ).

addition, at least initially, the water pushed up by the plunging jet apparently arises from the previously undisturbed water. Such a mechanism is quite consistent with (b) in figure 21.

Later on, the above-mentioned mechanism becomes less evident, and our impression is that, at least on certain pictures, some water originated from the

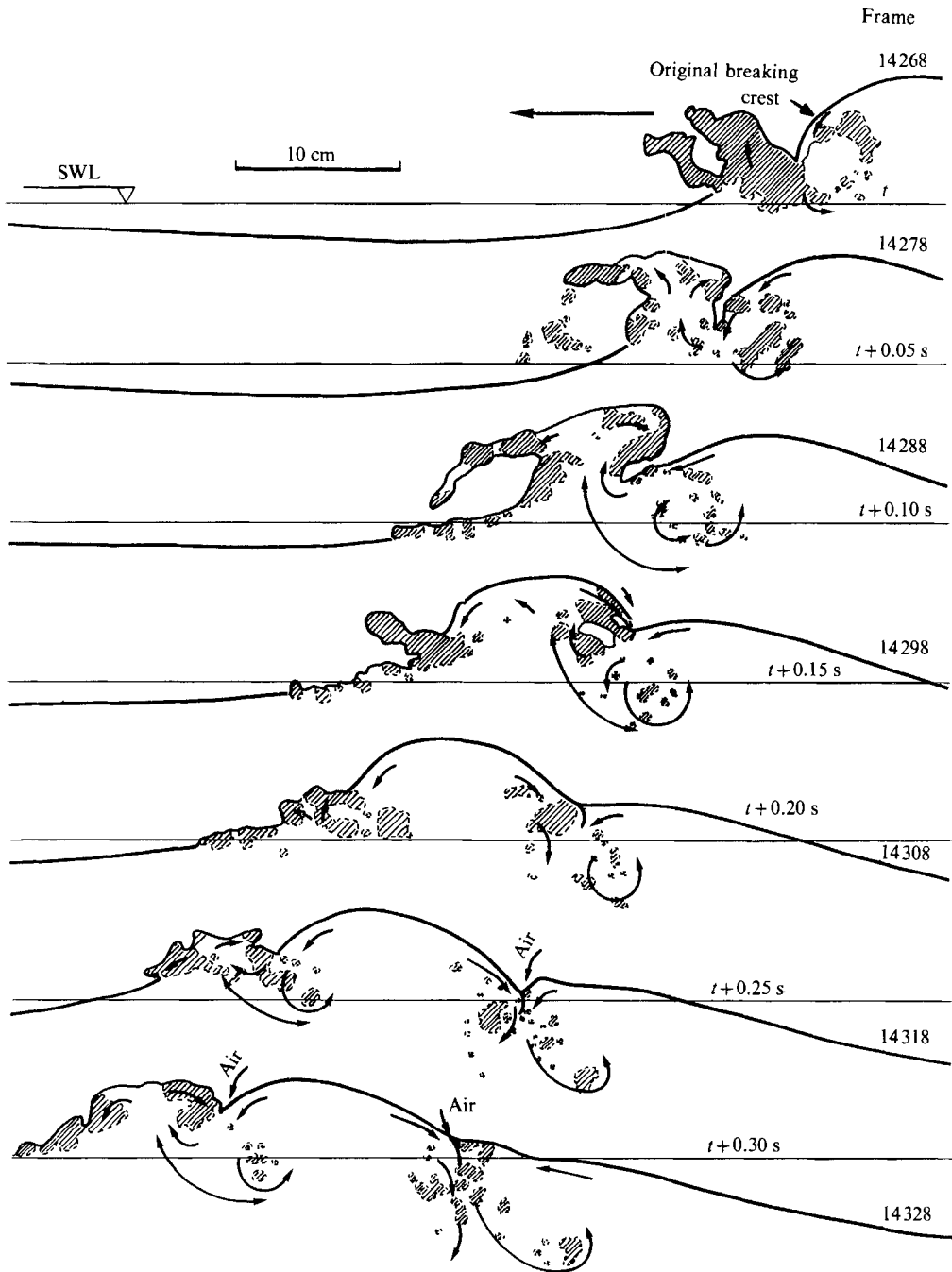


FIGURE 20. Generation and development of a second splash-up (cine camera frequency,  $24 \text{ f s}^{-1}$ ).

plunging crest becomes entrained in the splash-up, thus contributing to its development, and meaning that a process similar to the one indicated in (c) could, at a later time, play a role. The visualization technique we used does not allow a definitive confirmation of this impression, and further observations by means of appropriate visualization techniques are necessary.

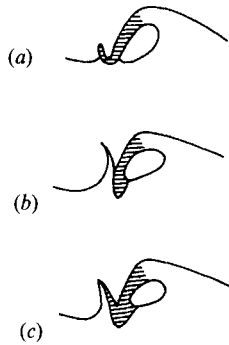


FIGURE 21. Possible modes of generation of the splash-up (from Peregrine 1983). Water in and from the falling jet is shaded.

The first splash-up can rise as high as the original plunging crest elevation (see figures 22 and 23). In agreement with the above-mentioned shallow-water observations by Jansen (1986*b*), when successive splash-ups are generated, their elevation decreases regularly from the first one to the last one (see figure 24): this decrease expresses the regular transformation of potential energy into kinetic energy happening during the breaking process at each successive splash-up cycle. This energy transformation leads to the formation of large vortices inside the splash-up and under the water surface, which generate regions of high turbulence visualized by the motion of air bubbles behaving like tracers.

With regard to the air-entrainment phenomenon, one can observe that the plunging breaking generates two successive processes: first, air is entrapped during the interaction between the plunging jet and the rear vortex of the splash-up, which looks like two water masses turning in opposite directions (see figures 19 and 20). It will be noticed that these two air entrainment processes can be observed at each successive splash-up cycle, the amount of air entrained decreasing logically from one splash-up to the next one.

This interaction between the breaking crest and the splash-up can display two modes: either the rear part of the splash-up flows over the falling crest, or the rear part of the splash-up looks like a falling water jet moving backwards and 'penetrating' the front of the original breaking crest as it moves forward (figure 25).

Observations of the spatial evolution of the splash-up showed that it can be projected at different angles: either forward or backward or straight up (see figures 19, 20 and 21). Such a tendency has been theoretically displayed by Peregrine (1981) who gave a mathematical description of the splash of a water jet falling on an originally undisturbed water layer.

#### 4.3.3. *The degenerated forward flow*

After the overturning and splash-up and vortex cycles, the forward region of the mixed air-water flow degenerates into a chaotic highly turbulent motion.

This flow displays a quasi-steady state for some time, the toe of this turbulent region running forward on the undisturbed water surface like a bore, with a celerity significantly higher than the celerity of the breaking crest and the splash-up celerity (see figure 26). The turbulent intensity of this chaotic air-water flow decreases with time and the water surface gradually again displays a smooth profile.

In plunging situations, a phenomenon sometimes appears that may be connected

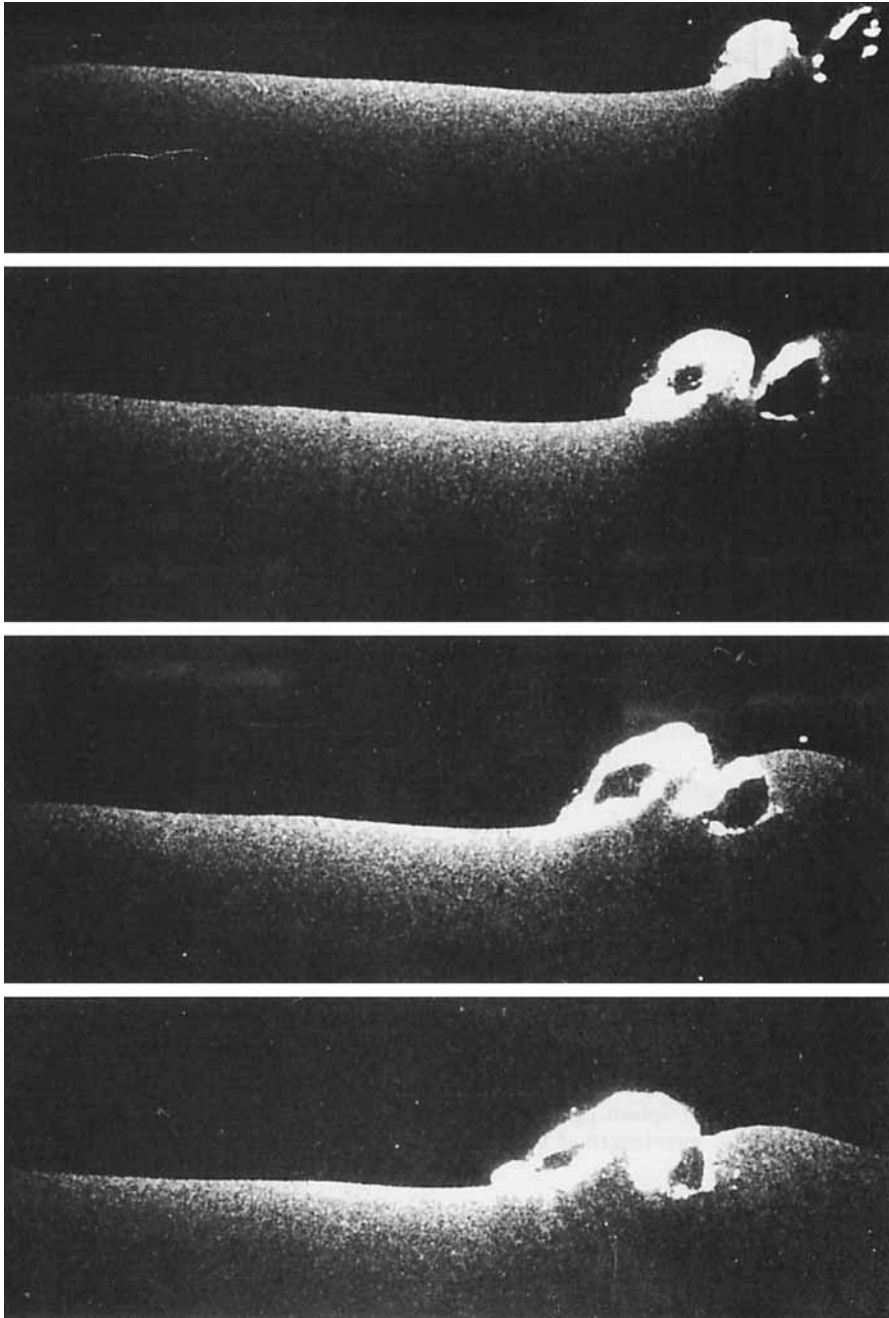


FIGURE 22. Series of photographs showing the occurrence and development of a splash-up (interframe time  $\approx 0.05$  s).

to the step by step potential energy dissipation occurring at each new splash-up cycle: the disappearing of the original breaking crest. After the breaking process has taken place, it will be observed at some time that the water surface displays a smooth profile without relief, as if a wave crest had never existed at this location (see figure 27). An interpretation may be that the potential energy of the original breaking wave

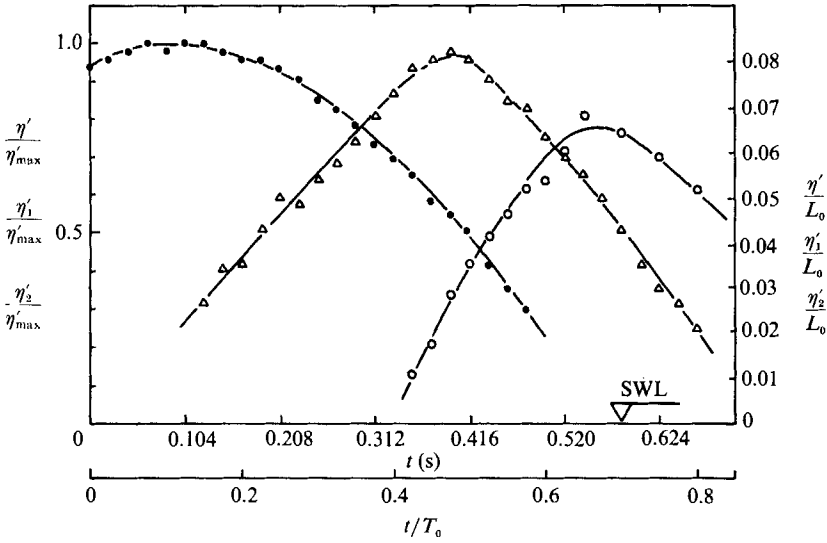


FIGURE 23. Breaking crest and splash-up elevations versus time during the breaking process: ●, breaking crest ( $\eta'$ );  $\Delta$ , first splash-up ( $\eta'_1$ );  $\circ$ , second splash-up ( $\eta'_2$ );  $T_0$ , wavemaker period;  $L_0$ , wavelength of the sinusoidal wave of  $T_0^{-1}$  frequency.

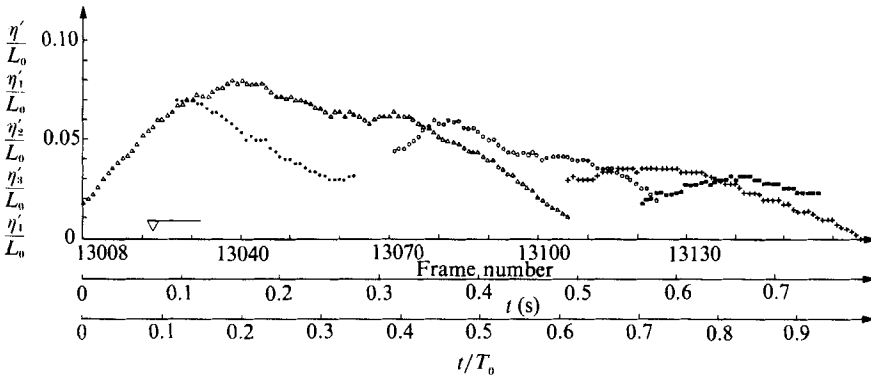
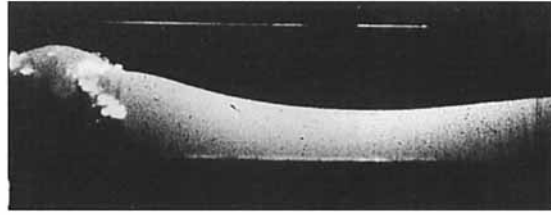
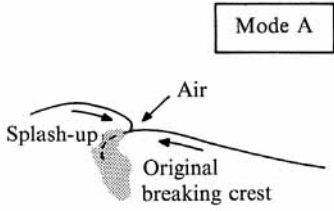


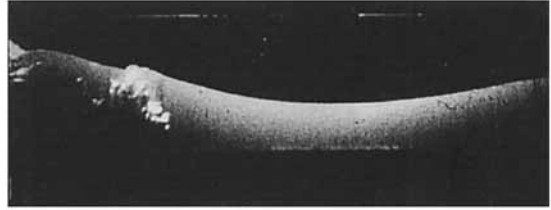
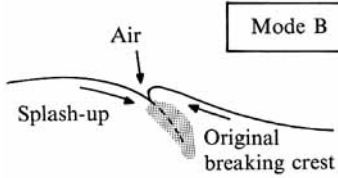
FIGURE 24. Regular decrease of successive splash-up elevation: ●, breaking crest ( $\eta'$ );  $\Delta$ , first splash-up ( $\eta'_1$ );  $\circ$ , second splash-up ( $\eta'_2$ ); +, third splash-up ( $\eta'_3$ ); ■, fourth splash-up ( $\eta'_4$ );  $T_0$ , wavemaker period;  $L_0$ , wavelength of the sinusoidal wave of  $T_0^{-1}$  frequency.

finally becomes wholly dissipated in the midst of the successive splash cycles; but no proof can be given, more especially as other phenomena connected to wave-wave interactions may also contribute to this disappearing. In any case this crest disappearance may contribute to the downshifting of modulated waves.

Finally, the decrease of the wave crest celerity during the breaking process, which can be qualitatively observed on the cine movies, was confirmed by measurements made on chronological series of pictures (figure 28). It will be noticed that the celerity of the crest, which, as expected, is higher than that of a linear wave before the onset of breaking, decreases after the crest touchdown point, and becomes significantly less than the celerity of a linear wave beyond this point.



Film BUL 11; Frame 1937



Film BUL 11; Frame 4466

FIGURE 25. The two modes of interaction between breaking crest and splash-up, and resulting air entrainment.

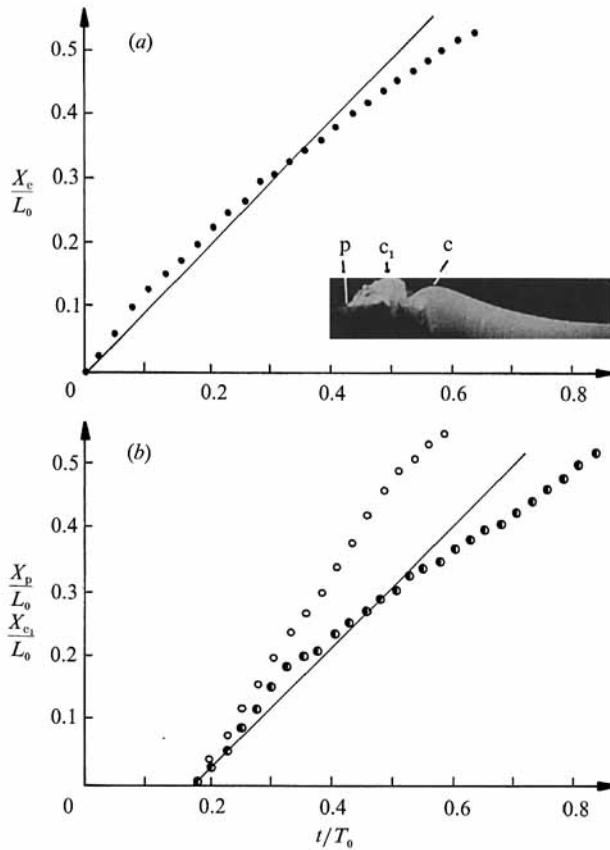


FIGURE 26. (a) Distance travelled by the crest of the original breaking crest ( $X_c$ ). (b) Distances travelled by the first splash-up crest ( $X_{c1}$ ), and the toe of the disturbed region ( $X_p$ ). ●, Original breaking crest; ○, first splash-up; ○, toe of the disturbed region. The distances have been scaled by the wavelength of a linear wave of  $T_0^{-1}$  frequency, where  $T_0$  denotes the wave generator period. —, linear wave. Time origin at breaking onset.

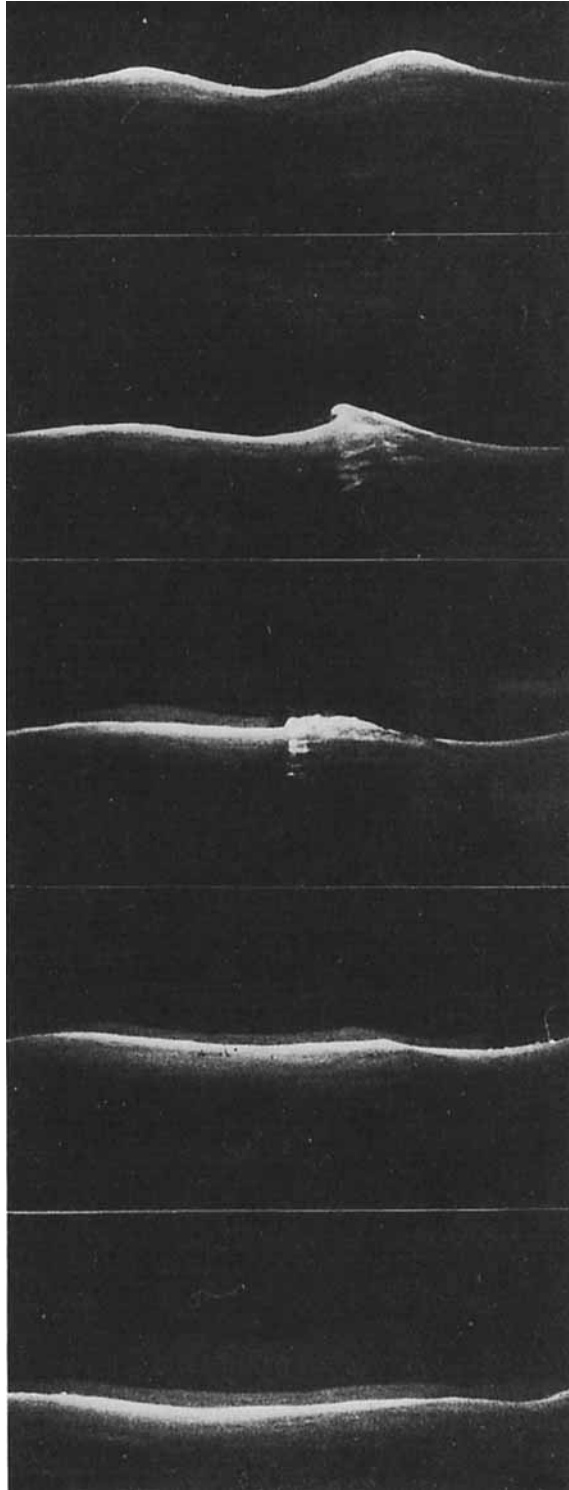


FIGURE 27. Almost complete dissipation of the crest potential energy observed during a breaking process (pictures from a moving camera). Width of the camera field  $\sim 1.40$  m. Time increasing from top to bottom (interframe time  $\approx 1$  s).

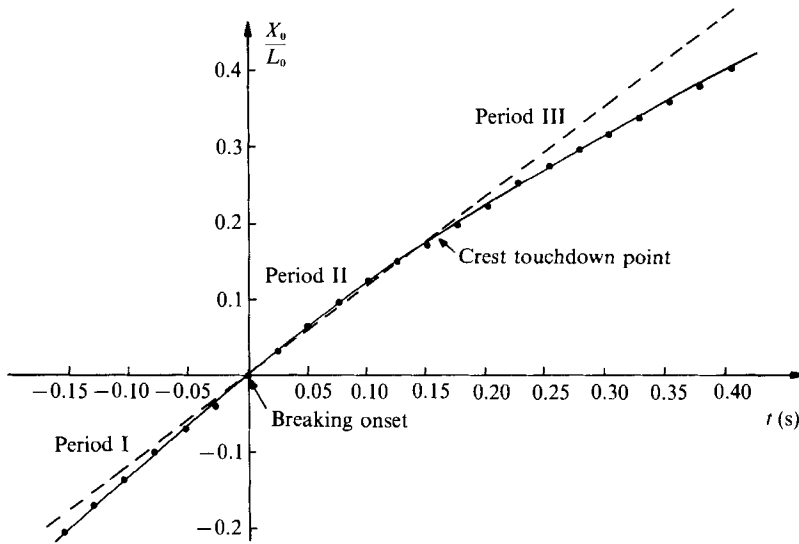


FIGURE 28. Breaking crest travel ( $X_0$ ): ---, linear wave; —●—, present experiment;  $L_0$ , length of the sinusoidal wave of  $T_0^{-1}$  frequency ( $T_0$ , wavemaker period).

## 5. Concluding remarks

Different geometric properties of a deep-water plunging breaker have been displayed by means of a simple visualization technique coupled to image analysis processing. Waves become more and more asymmetric during the prebreaking period, and the asymmetry has been measured quantitatively with several parameters. The asymmetry depends on the type of breaker: it is more marked for a plunging breaker than for a spilling one.

The significant asymmetry that a wave can display in the near-breaking region is an element to be taken into account in theoretical considerations. The relative disagreement between the theoretical Stokes' limiting wave height, valid for symmetric waves, and the experimental measurements, which appears in figure 4, supports this view. This asymmetry does appear, however, in certain theoretical computations.

A characteristic phenomenon occurring as the consequence of the interaction between the falling water jet and the undisturbed water surface, the so-called splash-up phenomenon, has been displayed. The elevation of the splash of water can rise as high as the original plunging crest. When several successive splash-up cycles occur, a gradual decrease of the potential energy from one cycle to the next is observed.

The splash-up phenomenon represents an aspect of the breaking process to be taken into consideration in a theoretical approach, in particular for energy dissipation estimation. But this is not easy to do because the understanding of this phenomenon, as well as knowledge of its consequences on turbulence generation and energy dissipation, are in their infancy.

Two modes of air entrainment by the plunging breaker were displayed: in the first mode, which is discussed here, air is entrapped under the falling water jet; in the second mode, air is entrapped during the meeting between the falling water jet and the vortex occurring at the rear of the splash-up. The non-negligible amount of air entrained by the second mode, connected to the important role played by air bubbles

in heat and mass transfer across the sea surface, emphasizes the necessity of an extensive knowledge of the splash-up phenomenon.

Finally, observation of plunging breakers can suggest a comparison with turbulent flows: the prebreaking region can be compared to a laminar stage, the breaking itself to a transient stage, and the afterbreaking region to a fully developed turbulent flow. If this comparison is adopted, it becomes evident that the experimental procedures and the theoretical and numerical approaches have to be adapted to these three different phases.

I am very grateful to Dr A. Ramamonjariosa and C. Kharif for the continued interest they have shown in this study. I wish to express my appreciation to Professor D. H. Peregrine for his encouragement and valuable suggestions. I gratefully acknowledge financial support provided by the Institut Francais de Recherche pour l'Exploitation de la Mer (IFREMER) and the Centre National de la Recherche Scientifique (CNRS). I also thank the Photographic and Cinematographic Laboratory in the Centre d'Essais de la Méditerranée (CEM) for its valuable technical help.

#### REFERENCES

- BIESEL, F. 1952 Study of wave propagation in water of gradually varying depth. *Natl Bur. of Stand. Circ.* 521, p. 243.
- COKELET, E. D. 1979 Breaking waves – the plunging jet and interior flow field. In *Mechanics of Wave Induced Forces on Cylinders* (ed. T. L. Shaw), p. 284. San Francisco: Pitman.
- DUNCAN, J. H. 1981 An experimental investigation of breaking waves produced by a towed hydrofoil. *Proc. R. Soc. Lond. A* 377, 331.
- DUNCAN, J. H. 1983 The breaking and non-breaking wave resistance of a two-dimensional hydrofoil. *J. Fluid Mech.* 126, 507.
- FLICK, R. E., GUZA, R. T. & INMAN, D. L. 1981 Elevation and velocity measurements of laboratory shoaling waves. *J. Geophys. Res.* 86, 4149.
- GALVIN, C. J. 1968 Breaker type classification on three laboratory beaches. *J. Geophys. Res.* 73, 3651.
- GALVIN, C. J. 1972 Wave breaking in shallow water, wave on beaches and resulting sediment transport. In *Waves on Beaches and Resulting Sediment Transport* (ed. R. E. Meyer), p. 413. Academic.
- GREENHOW, M. 1983 Free-surface flows related to breaking waves. *J. Fluid Mech.* 134, 259.
- HANSEN, J. B. & SVENDSEN, I. A. 1979 Regular waves in shoaling water, experimental data. *Inst. of Hydrodyn. Hydraul. Eng. Techn. Univ. Denmark*, Paper 21.
- HEDGES, T. S. & KIRKGOZ, M. S. 1981 An experimental study of the transformation zone of plunging breakers. *Coastal Engng* 4, 319.
- HOTTA, S. & MIZUGUCHI, M. 1980 A field study of waves in the surf zone. *Coastal Engng Japan* 23, 59.
- IVERSEN, H. W. 1953 Waves and breakers in shoaling water. In *Proc. 3rd Conf. on Coastal Eng., Council on wave research Berkeley*, chap. 1, p. 1.
- JANSEN, P. A. 1986a The period-doubling of gravity-capillary waves. *J. Fluid Mech.* 172, 531.
- JANSEN, P. A. 1986b Laboratory observations of the kinematics in the aerated region of breaking waves. *Coastal Engng* 9, 453.
- KHARIF, C. 1983 Calcul numérique de la déformation d'une onde de surface. *Rapport DRET/IMST* 83/366.
- KJELDSSEN, S. P. & MYRHAUG, D. 1978 Kinematics and dynamics of breaking waves. *Rep. STF60 A78100, Ships in Rough Seas*, Part 4. Norwegian Hydrodynamic Laboratories, Trondheim, Norway.

- KJELDSEN, S. P. & MYRHAUG, D. 1979 Wave-wave interactions and wave-current interactions in deep water. *Proc. 5th POAC Conf. Trondheim*, vol. III, p. 179.
- KOGA, M. 1986 Characteristic features of wind wave field with occasional breaking, and splashing droplets at high winds. In *Oceanic Whitecap and the Role in Air-Sea Exchange Processes* (ed. E. C. Monahan & G. McNiocail), p. 129. D. Reidel.
- LONGUET-HIGGINS, M. S. 1980 On the forming of sharp corners at a free surface. *Proc. R. Soc. Lond. A* **371**, 453.
- LONGUET-HIGGINS, M. S. 1982 Parametric solutions for breaking waves. *J. Fluid Mech.* **121**, 403.
- LONGUET-HIGGINS, M. S. 1983 Rotating hyperbolic flow: particle trajectories and parametric representation. *Q. J. Appl. Maths* **36**, 247.
- LONGUET-HIGGINS, M. S. & COKELET, E. D. 1976 The deformation of steep surface waves on water. I: A numerical method of computation. *Proc. R. Soc. Lond. A* **350**, 1.
- LONGUET-HIGGINS, M. S. & COKELET, E. D. 1978 The deformation of steep surface waves on water. II: Growth of normal-mode instabilities. *Proc. R. Soc. Lond. A* **364**, 1.
- LONGUET-HIGGINS, M. S. & FOX, M. J. H. 1978 Theory of the almost highest wave. Part 2. Matching and analytic extension. *J. Fluid Mech.* **85**, 769.
- MCIVER, P. & PEREGRINE, D. H. 1981 Comparison of numerical and analytical results for waves that are starting to break. *Hydrodynamics in Ocean Engineering*, p. 203. Norv. Inst. Techn.
- MASON, M. A. 1952 Some observations of breaking waves. *Gravity Waves. Natl Bur. Stand. Circ.* **521**, p. 215.
- MELVILLE, W. K. 1982 The instability and breaking of deep-water waves. *J. Fluid Mech.* **115**, 165.
- MERLIVAT, I. & MEMERY, L. 1983 Gas exchange across an air-water interface: Experimental results and modeling of bubble contribution to transfer. *J. Geophys. Res.* **88**, 707.
- NEW, A. L. 1983 A class of elliptical free-surface flows. *J. Fluid Mech.* **130**, 219.
- OCHI, M. K. & TSAI, C. H. 1983 Prediction of occurrence of breaking waves in deep water. *J. Phys. Oceanogr.* **13**, 2008.
- PEREGRINE, D. H. 1981 The fascination of fluid mechanics. *J. Fluid Mech.* **106**, 59.
- PEREGRINE, D. H. 1983 Breaking waves on beaches. *Ann. Rev. Fluid Mech.* **15**, 149.
- PEREGRINE, D. H., COKELET, E. D. & MCIVER, P. 1980 The fluid mechanics of waves approaching breaking. *Proc. 17th Conf. Coastal Engng.* ASCE.
- PRICE, R. K. 1971 The breaking of water waves. *J. Geophys. Res.* **76**, 1576.
- RAMBERG, S. E., BARBER, M. E. & GRIFFIN, O. M. 1985 Laboratory studies of steep and breaking deep water waves in a convergent channel. *NRL Rep.* 5610.
- RAMBERG, S. E. & GRIFFIN, O. M. 1986 A laboratory study of steep and breaking deep water waves. *Proc. ASCE. J. Waterways, Port, Coastal Ocean Div.* **113**, 493.
- SCHULTZ, W. W. 1985 Integral equation algorithm for breaking waves. *Proc. Eleventh IMACS World Congress, Oslo*, vol. 2, p. 219.
- STOKES, G. G. 1880 Considerations relative to the greatest height of oscillatory irrotational waves which can be propagated without change of form. *Mathematical and Physical Papers*, vol. 1, p. 225.
- SU, M. Y., BERGIN, M., MARLER, P. & MYRICK, R. 1982 Experiments on nonlinear instabilities and evolution of steep gravity-wave trains. *J. Fluid Mech.* **124**, 45.
- SUHAYDA, J. N. & PETTIGREW, N. R. 1977 Observations of wave height and wave celerity in the surf zone. *J. Geophys. Res.* **82**, 1419.
- VAN DORN, W. G. 1978 Breaking invariants in shoaling waves. *J. Geophys. Res.* **83**, 2981.
- VAN DORN, W. G. & PAZAN, S. E. 1975 Laboratory investigation of wave breaking. *Scripps Institution of Oceanography Rep.* 75-21, AD A013 336.
- VINJE, T. & BREVIK, P. 1981a Breaking waves on water of finite depth. A numerical study. *Ship Research Institute of Norway, Rep.* R-111-81.
- VINJE, T. & BREVIK, P. 1981b Numerical simulation of breaking waves. *Adv. Water Resources* **4**, 77.